Solar Energy Materials & Solar Cells 128 (2014) 57–68

Contents lists available at ScienceDirect

Solar Energy Materials & Solar Cells

journal homepage: www.elsevier.com/locate/solmat

Bifacial *n*-type silicon solar cells for upconversion applications

Marc Rüdiger [a], Stefan Fischer [a], Judith Frank [a], Aruna Ivaturi [b], Bryce S. Richards [b,c,d], Karl W. Krämer [e], Martin Hermle [a], Jan Christoph Goldschmidt [a,f,*]

[a] Fraunhofer Institute for Solar Energy Systems (ISE), Heidenhofstrasse 2, 79110 Freiburg, Germany
[b] School of Engineering and Physical Sciences, Heriot-Watt University, Edinburgh, EH14 4AS, Scotland, United Kingdom
[c] Institute of Microstructure Technology (IMT), Karlsruhe Institute of Technology, Hermann-von-Helmholtz-Platz 1, 76344 Eggenstein-Leopoldshafen, Germany
[d] Light Technology Institute (LTI), Karlsruhe Institute of Technology, Engesserstrasse 13, Building 30.34, 76131 Karlsruhe, Germany
[e] Department of Chemistry and Biochemistry, University of Bern, Freiestrasse 3, 3012 Bern, Switzerland
[f] Imperial College, Department of Physics, South Kensington Campus, London SW7 2AZ, United Kingdom

ARTICLE INFO

Article history:
Received 13 January 2014
Received in revised form
7 May 2014
Accepted 9 May 2014
Available online 29 May 2014

Keywords:
Upconversion
Bifacial solar cells
Efficiency limits
n-type silicon solar cells
Anti-reflection coatings

ABSTRACT

Upconversion of sub-band-gap photons has the potential to increase the efficiency of solar cells significantly, but requires modification of the solar cells. In this paper, we present a calculation framework to assess the efficiency of a combined bifacial silicon solar cell upconverter device, which is then used to optimize the solar cell's front and rear side anti-reflection coatings. Our calculations show that an upconverter can increase the efficiency of an optimized solar cell by 3.0% relative. Subsequently, planar bifacial *n*-type silicon solar cells were fabricated with optimized anti-reflection coatings. An upconversion layer – containing the upconverter phosphor β-$NaY_{0.8}Er_{0.2}F_4$ embedded in the polymer perfluorocyclobutyl – was attached to the rear side of the solar cells and an external quantum efficiency arising from the upconversion of sub-band-gap photons of 1.69% was measured under 1508 nm monochromatic excitation with an irradiance of 1091 W/m^2. This corresponds to a value of 0.15 (W/cm^2)$^{-1}$ when normalized to the irradiance, constituting a five-fold increase compared to the previously best published normalized values that were achieved without optimized solar cells.

1. Introduction

Solar cells made from materials with one single band-gap do not fully utilize the solar spectrum. Silicon (Si) photovoltaic (PV) devices fail to capture about 20% of the incident energy, with sub-band-gap photons being not effectively harvested. Upconversion (UC) of such sub-band-gap photons can minimize these losses [1,2] and high efficiency gains due to the application of upconverters to Si solar cells have been theoretically predicted [1,3,4]. The theoretical limit for the efficiency of a Si solar cell (band-gap 1.117 eV) with additional upconverter, illuminated by non-concentrated light, is reported to be 40%, compared to a radiative limit efficiency of the solar cell alone of 33.25% [4]. However, while a 20% relative increase in efficiency due to the addition of an upconverter is predicted, experimental results have demonstrated only very small increases in overall device efficiency [5–7]. Shalav et al. investigated bifacial Si solar cells, with an upconverter layer containing microcrystalline hexagonal sodium yttrium fluoride doped with 20% erbium ions, β-$NaY_{0.8}Er_{0.2}F_4$, attached to the rear side. They reported an external quantum efficiency (EQE) of the combined upconverter Si solar cell device of 3.4% under monochromatic excitation with a wavelength of 1523 nm and an irradiance of 24,000 W/m^2 [8]. The upconversion quantum yield, and consequently also the EQE of a system that utilizes sub-band-gap photons by upconversion, increases with the incident irradiance. Therefore, efficiency values are commonly normalized to the irradiance to make the values more comparable [9]. The values reported by Shalav et al. correspond to a normalized efficiency of 0.014 (W/cm^2)$^{-1}$ (the unit of the normalized efficiency is also commonly written as cm^2/W in literature) [5]. Fischer et al., using the same UC material, determined an EQE of 0.34% for an excitation wavelength of 1523 nm and a considerably lower monochromatic irradiance of 1090 W/m^2, resulting into a higher normalized value of 0.03 (W/cm^2)$^{-1}$[6].

Many challenges need to be overcome in order to realize a successful upconversion photovoltaic device (UC PV device), including the development of highly efficient upconverter materials [6–8,10] that can achieve good performance under realistic irradiance values. In addition, another key reason for the low performance that has not been examined yet is that the solar cells used in the experimental works were not adapted to the application of an UC layer at the rear [5–8]. In this work, we address the

* Corresponding author. Tel.: +49 761 4588 5475; fax: +49 761 4588 9250.
E-mail address: jan.christoph.goldschmidt@ise.fraunhofer.de (J.C. Goldschmidt).

http://dx.doi.org/10.1016/j.solmat.2014.05.014
0927-0248/

question how crystalline Si solar cells can be adapted to maximize the overall efficiency by the addition of an upconverter system. In this context, the ideal solar cell should fulfill three criteria: firstly, the solar cell should have a very high transmittance for photons with wavelengths $\lambda > 1200$ nm in order to illuminate the UC layer located on the rear side of the device. Secondly, the solar cell should have a high EQE when illuminated from the rear with photons emitted by the upconverter. These two requirements mean that the solar cell needs to have an adapted, bifacial functionality. Thirdly, the solar cell itself needs to have a high overall efficiency to ultimately optimize the UC PV device.

The increased transmission can be achieved by adapted anti-reflection coatings (ARCs). An early work describing the optimization of single- and double-layer ARCs considering as well the need for effective surface passivation can be found in Ref. [11]. In the context of spectral management, ARCs have been optimized for the emission for organic dyes, for example in Refs. [12,13]. In Ref. [5], the use of adapted ARCs was suggested to increase UC efficiencies, but no devices with optimized ARC have been fabricated yet.

In the first part of this work, we focus on the optimization of ARCs and present a simulation framework that allows us to assess the performance of solar cells with attached upconverter. The framework includes the simulation of the solar cell performance under standard front side illumination, the optical properties of the solar cell that determine the illumination of the upconverter, a parameter model of the upconverter behavior, and the performance of the solar cell under rear-side illumination from the upconverter.

The model of the upconverter is based on the widely used β-$NaY_{0.8}Er_{0.2}F_4$ phosphor, which exhibits efficient UC luminescence predominantly at 980 nm when excited with wavelengths around $\lambda = 1523$ nm [6,14–16]. One disadvantage of this upconverter material is that it only utilizes a 100 nm wide spectral range efficiently. Therefore, we assume the use of a second idealized luminescent material that has a broad absorption spectrum and emits in the absorption range of the upconverter as suggested by Strümpel et al. [17], a concept also called spectral concentration. Furthermore, we assume a system geometry, in which this luminescent material is embedded in a transparent matrix forming a luminescent solar concentrator (LSC) that allows for additional geometric concentration onto the upconverter that covers only a fraction of the LSC surface, a configuration proposed by Goldschmidt et al. [3,18]. The suggested setup is shown in Fig. 1.

For the simulation of solar cell characteristics, commercial simulation tools exist that achieve high accuracy, such as the Sentaurus TCAD [19] used in this work. Solar cells made on *n*-type Si have been already simulated successfully. To describe the effects of upconversion, the existing simulation models for *n*-type Si silicon solar cells [20–25], need to be extended to include rear-side illumination. This was successfully implemented for a different purpose in an earlier work [26,27]. Additionally, the covered spectral range was extended to wavelength beyond 1200 nm, a spectral region that is typically not covered in Si solar cell simulations. This included determining all necessary parameters, especially the optical dispersion curves for the used materials, also for the wavelength range above 1200 nm [27].

The combined simulation model is subsequently used to optimize the optical properties of the solar cell and to calculate the additional current density from UC. This allows for an assessment of the potential efficiency increase due to upconversion, based on realistic solar cell properties and realistic upconverter characteristics in combination with idealized assumptions for the extension of the used spectral range. This extends earlier work [4,28], where realistic solar cell properties were combined with ideal upconverter properties. These optimizations are carried out both for planar and both-sides-textured solar cells. Both-sides-textured solar cells were chosen, because the texturing promises advantageous anti-reflection properties. Planar solar cells were included, as all previous experimental results were achieved on planar solar cells, motivated by the higher transmission of upconvertible light in the planar case.

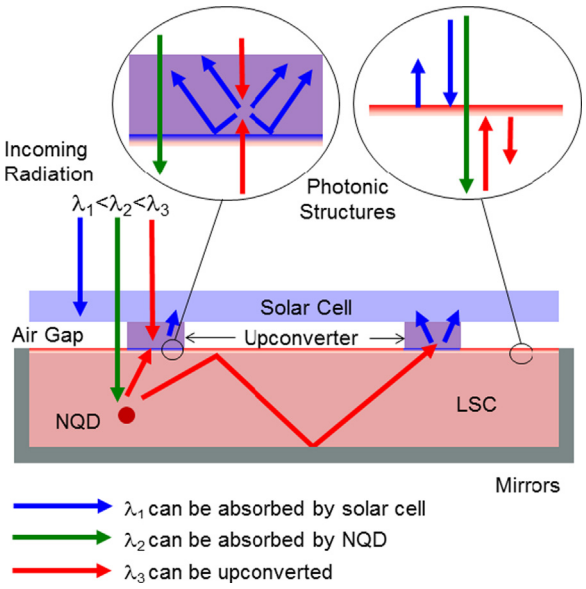

Fig. 1. Concept of an advanced upconverter system [3,18]. It consists of a bifacial solar cell that can utilize higher energy photons (λ_1), and of an upconverter that can convert low energy photons (λ_3) into higher energy photons (λ_1). Photons of the intermediate spectral range (λ_2) are absorbed by luminescent nanocrystalline quantum dots (NQD), which are embedded in a transparent matrix. The luminescent NQD emit photons that can be utilized by the upconverter (λ_3). The emitted photons are guided by total internal reflection and photonic structures to the upconverter elements. Such a configuration increases the photon flux in the absorption range of the upconverter (spectral concentration). Additional geometric (or spatial) concentration occurs because the upconverter does not cover the full solar cell area. Spectrally selectively reflecting photonic structures ensure that the photons are directed to that part of the system, in which they are used most efficiently.

The second part of the paper deals with the fabrication and characterization of optimized, planar solar cells that were prepared based on the findings presented in the first part. Upconverter samples are applied to different kind of solar cells, and the EQE of the whole system of upconverter and solar cell is measured under monochromatic excitation at 1508 nm, showing extremely high performance. The purpose of these measurements is to document the successful optimization carried out in the first part of the paper. Detailed experimental investigations of UC PV devices using our optimized solar cells focusing on the upconverter materials and different illumination conditions (monochromatic, broad-band) have been performed in the mean-time, achieving as well record breaking results [29,30].

2. Optimizing the solar cell structure

2.1. Solar cell simulation model and figures-of-merit

The optical performance of the solar cell was modeled using Sentaurus TCAD [19]. The optical properties of the ARCs were determined via transfer matrix calculations and these data were implemented into the Sentaurus ray-tracing tool. One important effect determining the transmission of sub-band-gap photons is free carrier absorption (FCA). FCA was considered in the simulations based on the parameterization of Green [33]. In the

simulation, 200 μm 1 Ω cm *n*-type silicon, a boron doped emitter profile featuring a sheet resistance of $R_{sh}=130\,\Omega$/sq, and a phosphorus doped BSF profile with $R_{sh}=19\,\Omega$/sq were assumed, which corresponds to the parameters of the realized solar cells. Front- and rear-side illumination of the solar cell were treated independently, as described in Refs. [26,31]. Firstly, the depth profile of the generation of free charge carriers due to the absorption of photons (absorption profile) in the solar cell precursor structures without contact grids and the number of transmitted photons was determined using the air-mass 1.5 global (AM1.5G) solar spectrum (IEC 60904-3 [32]) at normal incidence. Subsequently, the absorption profile due to the light emitted by the upconverter was determined, with isotropic emission of the upconverter being assumed. The modeling of the upconverter behavior will be discussed in detail in Section 2.2.

Three figures-of-merit were defined in order to properly assess the performance of different device designs with regard to solar cell efficiency, performance of the upconverter, and overall system performance. The first one is Abs_0, the fraction of incident photons that are absorbed by the solar cell without an upconverter being present, defined as

$$Abs_0=\frac{\Phi_{abs,0}}{\Phi_{in}}=\frac{\int_{280\ nm}^{4000\ nm} Abs(\lambda)\mathrm{AM1.5G_{ph}}(\lambda)d\lambda}{\int_{280\ nm}^{4000\ nm} \mathrm{AM1.5G_{ph}}(\lambda)d\lambda} \quad (1)$$

where Φ_{in} indicates the photon flux density incident onto the solar cell, $\Phi_{abs,0}$ the absorbed photon flux density (without an upconverter), $\mathrm{AM1.5G_{ph}}(\lambda)$ is the spectral incident photon flux density from the sun, and $Abs(\lambda)$ denotes the spectrally resolved absorptance, as determined in the described numerical simulation. $Abs(\lambda)$ only includes absorption in the Si part of the investigated structure, and not parasitic absorption in passivation layers or ARCs, which has been considered in the simulation.

The second figure-of-merit is *Trans*, the fraction of incident photons that are transmitted and that have sufficient energy for UC. In this paper, we perform calculations for the upconverter β-$NaY_{0.8}Er_{0.2}F_4$. In Ref. [6], it was shown that β-$NaY_{0.8}Er_{0.2}F_4$ has its peak upconversion quantum yield (QY) at 1523 nm, and that for a wavelength range from 1490 to 1550 nm the upconversion quantum yield is at least half the peak value. Thus, in this paper we define the active region of the upconverter to be 1490 to 1550 nm and consequently, the upper wavelength limit of 1550 nm is used in the spectral integration. We define *Trans* as

$$Trans=\frac{\Phi_{trans}}{\Phi_{in}}=\frac{\int_{280\ nm}^{1550\ nm} T(\lambda)\mathrm{AM1.5G_{ph}}(\lambda)d\lambda}{\int_{280\ nm}^{4000\ nm} \mathrm{AM1.5G_{ph}}(\lambda)d\lambda}, \quad (2)$$

where Φ_{trans} is the transmitted flux density of photons with wavelengths shorter than 1550 nm, and $T(\lambda)$ the spectrally resolved transmittance.

The third figure-of-merit is Abs_{total}, which is the overall absorbed photon flux density Φ_{abs} being absorbed in the solar cell in a combined upconverter solar cell system, normalized to the overall incident photons flux density Φ_{in}:

$$Abs_{total}=\frac{\Phi_{abs}}{\Phi_{in}}=Abs_0+Abs_{UC}. \quad (3)$$

it is composed of two terms: Abs_0, the fraction of photons being absorbed by the solar cell without the upconverter being present; and Abs_{UC}, the photon flux density emitted by the upconverter and absorbed in the solar cell, normalized to the overall incident photon flux density. The method for calculating the number of photons being emitted by the upconverter, and determination of the subsequent absorption in the solar cell, is presented in detail in the following section. It is clear, however, that for an overall device optimization Abs_{total} has to be maximized. Abs_{total}, Abs_0 and Abs_{UC} can be converted to equivalent currents that could be expected from the solar cell, if all photons absorbed in the Si would generate a free charge carrier that is collected at the appropriate contacts, $J_{sc,total}$, $J_{sc,0}$ and $J_{sc,UC}$ via

$$J_{SC,total/0/UCl}=qAbs_{total/0/UC}\Phi_{in}, \quad (4)$$

with q being the elementary charge.

2.2. Modeling the impact of upconversion on solar cell performance

The figure-of-merit Abs_{UC} combines properties of the upconverter and of the solar cell. It can be expressed as

$$Abs_{UC}=Abs_{rear}\cdot Trans\cdot eUCQY(I_{inc,UC}). \quad (5)$$

In this relation, Abs_{rear} is the average probability that a photon emitted by the upconverter is absorbed in the Si part of the investigated structure. The β-$NaY_{0.8}Er_{0.2}F_4$ exhibits a dominant luminescence band around 980 nm due to a two-step UC process, while luminescence resulting from higher energy Er^{3+} transitions contribute less than 1% to the emission of upconverted photons for low power excitation [6]. The peak at 980 nm has a full-width at half-maximum (FWHM) of about 30 nm. We use the absorption probability Abs_{rear} calculated by our numerical model for photons with a wavelength of 980 nm for all emitted photons. Thereby, we neglect any effects of a more complex emission spectrum. The emission was assumed to be isotropic and the refractive index of the upconverter to be $n=1.5$ as determined in [34]. *Trans* is the fraction of incident photons that are transmitted, as defined above. Finally, $eUCQY(I_{inc,UC})$ is the average external upconversion quantum yield, describing the fraction of the transmitted photons reaching the upconverter that are converted into photons with energies above the band gap of Si. Please note that $eUCQY(I_{inc,UC})$ depends on the irradiance $I_{inc,UC}$ that illuminates the upconverter.

In principle, $eUCQY(I_{inc,UC})$ is known from experiments. In [6] it was shown that for an monochromatic excitation at 1523 nm $eUCQY_{1523\ nm}(I_{inc,UC})$ increases with irradiace $I_{inc,UC}$ onto the upconverter and the dependence can be described with a power law

$$eUCQY_{1523\ nm}(I_{inc,UC})=c_1 I_{inc,UC}^{m-1}+c_2. \quad (6)$$

For irradiance values between 0 and 490 W/m^2 the characteristic exponent was found to be $m=1.86\pm0.03$, and the other parameters were $c_1=(1.1\pm0.2)\times10^{-4}$ and $c_2=(-4.7\pm1.5)\times10^{-4}$. For higher irradiance values between 440 and 1050 W/m^2 the characteristic exponent was found to be $m=1.35\pm0.04$, with the other parameters $c_1=(6.0\pm2.0)\times10^{-3}$ and $c_2=(-3.2\pm0.7)\times10^{-2}$ [6]. For a monochromatic irradiance of 1050 W/m^2, for example, this results in an $eUCQY(I_{inc,UC})$ of 3.7%.

For the assessment of the overall system performance, however, broad-band illumination by the transmitted spectrum has to be taken into account. As stated above, we define the active region of efficient upconversion to range from 1490 nm to 1550 nm for the investigated β-$NaY_{0.8}Er_{0.2}F_4$. The experimental analysis of this material under broad band illumination and the modeling of broad band illumination and upconversion are on-going work [30], and only a few results have been published yet [6–8,10,29,30,35].

As already mentioned in the introduction, it is desirable to extend the used spectral range of the upconverter such that a larger fraction of the solar spectrum can be utilized. This can be achieved with a second luminescent material that absorbs over a broad spectral range and emits in the narrow absorption range of the upconverter. For our calculations, we assume the advanced upconverter system depicted in Fig. 1. In such an advanced system, a complex sequence of events occurs, which is not sensible to cover in detail for the optimization of the solar cells. For simplification, we assume that all photons, which are transmitted by the

Table 1
Overview of determined optimum individual layer thicknesses d_{opt} in DLARCs made of either a-SiN_x:H/SiO_2, a-SiN_x:H/MgF_2 or TiO_2/MgF_2 for planar and solar cells textured on both sides, as determined for the two different optimization scenarios $Cell_{opt}$ (highest Abs_0) and UC_{opt} (highest *Trans*). Additionally, the resulting figures-of-merit Abs_0, $J_{sc,0}$, *Trans*, Abs_{UC}, $J_{sc,UC}$, Abs_{total}, $J_{sc,total}$, and the relative increase in projected current $J_{sc,UC}/J_{sc,0}$ are presented, all calculated for the case of a high concentration factor $K=100$.

	1st layer		2nd layer		*Figures of merit*							
	Material	d_{opt} [nm]	**Material**	d_{opt} [nm]	Abs_0 [%]	$J_{sc,0}$ [mA/cm^2]	*Trans* [%]	Abs_{UC} [%]	$J_{sc,UC}$ [mA/cm^2]	Abs_{total} [%]	$J_{sc,total}$ [mA/cm^2]	$J_{sc,UC}/J_{sc,0}$ [%]
Planar												
$Cell_{opt}$	TiO_2	50	MgF_2	90	47.0	32.5	19.2	1.78	1.23	48.8	33.8	3.79
UC_{opt}	TiO_2	100	MgF_2	120	43.6	30.1	21.2	2.05	1.42	45.6	31.5	4.72
$Cell_{opt}$	a-SiN_x:H	50	MgF_2	80	52.9	36.6	18.8	1.74	1.20	54.7	37.8	3.28
UC_{opt}	a-SiN_x:H	110	MgF_2	90	48.4	33.5	21.2	2.05	1.42	50.4	34.9	4.23
$Cell_{opt}$	a-SiN_x:H	50	SiO_2	70	52.8	36.5	18.9	1.74	1.21	54.5	37.7	3.30
UC_{opt}	a-SiN_x:H	100	SiO_2	100	49.2	34.0	21.2	2.05	1.42	51.3	35.4	4.17
Textured both sides												
$Cell_{opt}$	TiO_2	40	MgF_2	80	58.8	40.6	16.1	1.75	1.21	60.5	41.8	2.98
UC_{opt}	TiO_2	100	MgF_2	140	57.6	39.8	16.7	1.85	1.28	59.4	41.1	3.21
$Cell_{opt}$	a-SiN_x:H	50	MgF_2	90	58.9	40.7	16.2	1.78	1.23	60.7	42.0	3.02
UC_{opt}	a-SiN_x:H	100	MgF_2	140	57.9	40.0	16.7	1.85	1.28	59.7	41.2	3.19
$Cell_{opt}$	a-SiN_x:H	40	SiO_2	80	59.1	40.8	16.2	1.77	1.22	60.8	42.1	2.99
UC_{opt}	a-SiN_x:H	100	SiO_2	120	58.2	40.2	16.7	1.85	1.28	60.1	41.5	3.18

solar cell with wavelengths $\lambda < 1550$ nm are either directly utilized by the upconverter or absorbed by the NQDs. Photons absorbed by the NQD are re-emitted in the absorption range of the upconverter with a QY of 100% (that is for each photon absorbed in the NQD one photon is emitted) and guided without losses to the upconverter. Additionally, we assume an $eUCQY(I_{inc,UC})$ of the upconversion similar to that measured at 1523 nm for the entire effective spectral range. These highly idealized assumptions lead to the simplification that all transmitted photons with $\lambda < 1550$ nm contribute to the upconversion with the same $eUCQY_{1523\ nm}$ ($I_{inc,UC}$), as given by Eq. (6). For irradiance values above 1050 W/m^2, which is greater than the specified range, the fit parameters of the higher irradiance range were used for extrapolation.

As can be seen in Fig. 1, the upconverter does not necessarily cover the complete active area of the solar cell, A_{SC}. The additional spatial concentration is accounted for by a concentration factor K, arising from the ratio between the total area of the solar cell A_{SC} and the surface area of the upconverter A_{UC}:

$$K = \frac{A_{SC}}{A_{UC}}. \tag{7}$$

Subsequently, the irradiance incident on the upconverter $I_{inc,UC}$ is given by

$$I_{inc,UC} = K\Phi_{trans}\frac{hc}{1550\ nm} \tag{8}$$

with h being the Planck constant and c the speed of light. This expression can then be used as input for Eqs. (5) and (6) to calculate Abs_{UC}.

2.3. Results of model-based optimization of anti-reflection coatings

The front side of the solar cell should have a low reflection in the entire wavelength range from $\lambda = 280$–1550 nm, such that the solar cell can use photons in the wavelength range below 1150 nm efficiently, and such that photons with longer wavelength have a chance to reach the upconverter. Since a single-layer ARC can only minimize the reflectance for one specific wavelength, it is advantageous to use a double-layer anti-reflection coating (DLARC) [11]. Therefore, we analyzed systems with two layers theoretically.

The optimization was carried out assuming air with $n=1$ as adjoining medium on the front. To enhance the surface passivation, all investigated structures feature a 10 nm thick aluminum oxide (Al_2O_3) layer between the Si and the inner ARC. Al_2O_3 saturates dangling bonds at the Si surface very well and features a strong negative surface charge density of -9.9 × 10^{13} cm^{-3} [36] for ideal passivation of boron-doped surfaces [37,38]. Al_2O_3 shows as well good passivation qualities on lowly phosphorus-doped surfaces [39] at an illumination intensity of 1 sun. Due to the thinness of the Al_2O_3 layer, it has a minor effect on the optical properties.

Promising material combinations are layer systems with hydrogenated amorphous silicon nitride (a-SiN_x:H) as the first high-n layer, with $n=1.99$, and silicon dioxide (SiO_2, $n=1.47$) or magnesium fluoride (MgF_2, $n=1.39$) as the second low-n layer. An alternative material combination is amorphous titanium dioxide (TiO_2) with a refractive index of $n=2.07$ in combination with MgF_2. All refractive indices reported here are for $\lambda = 1000$ nm. However, dispersion curves reported in [27] covering the whole considered range were used in the simulation. They can be found in the supplemental material in Fig. 1S.

We performed optimization runs for all mentioned material systems. A summary of the results is presented in Table 1. The highest simulated Abs_{total} for planar solar cells was found for the a-SiN_x:H /MgF_2 material systems. As we will see later on, also the highest EQE_{UC} was measured for this material system. Therefore, results for this material system will be presented in detail in the following sections for planar solar cells (Section 2.3.1) and for solar cells textured on both sides (Section 2.3.2), while only core results for the other material systems will be given. Detailed simulation results for the other material systems can be found in the Supplemental material.

For the following simulation concerning the optimization of the front side DLARC, the Si wafer thickness was 180 μm, and a

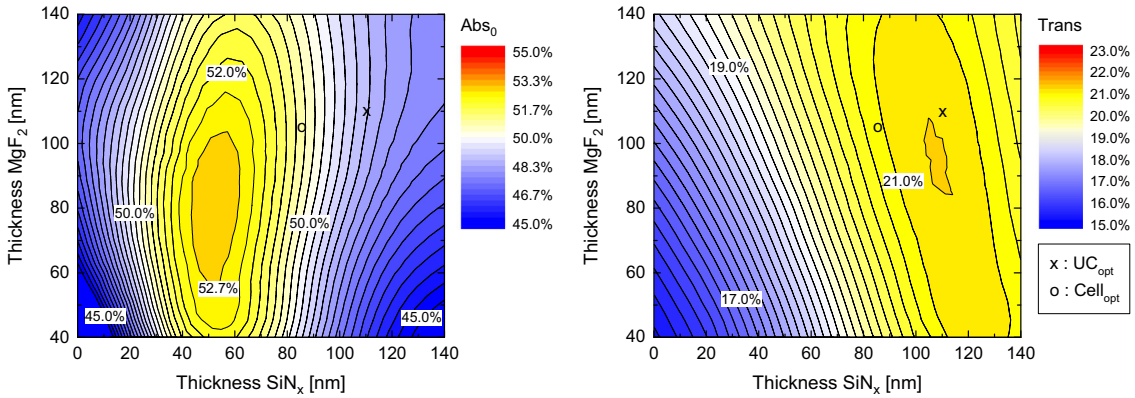

Fig. 2. Effect of layer thicknesses variations on Abs_0 (left) and *Trans* (right) for a-SiN_x:H and MgF_2 stack as DLARC for the front side of a planar bifacial Si solar cell. The optimum layer thicknesses for Abs_0 are thinner than for high *Trans*. Experimentally realized layer thicknesses are indicated with a circle ($Cell_{opt}$), or cross (UC_{opt}). Due to a processing error they differ from the originally anticipated optima.

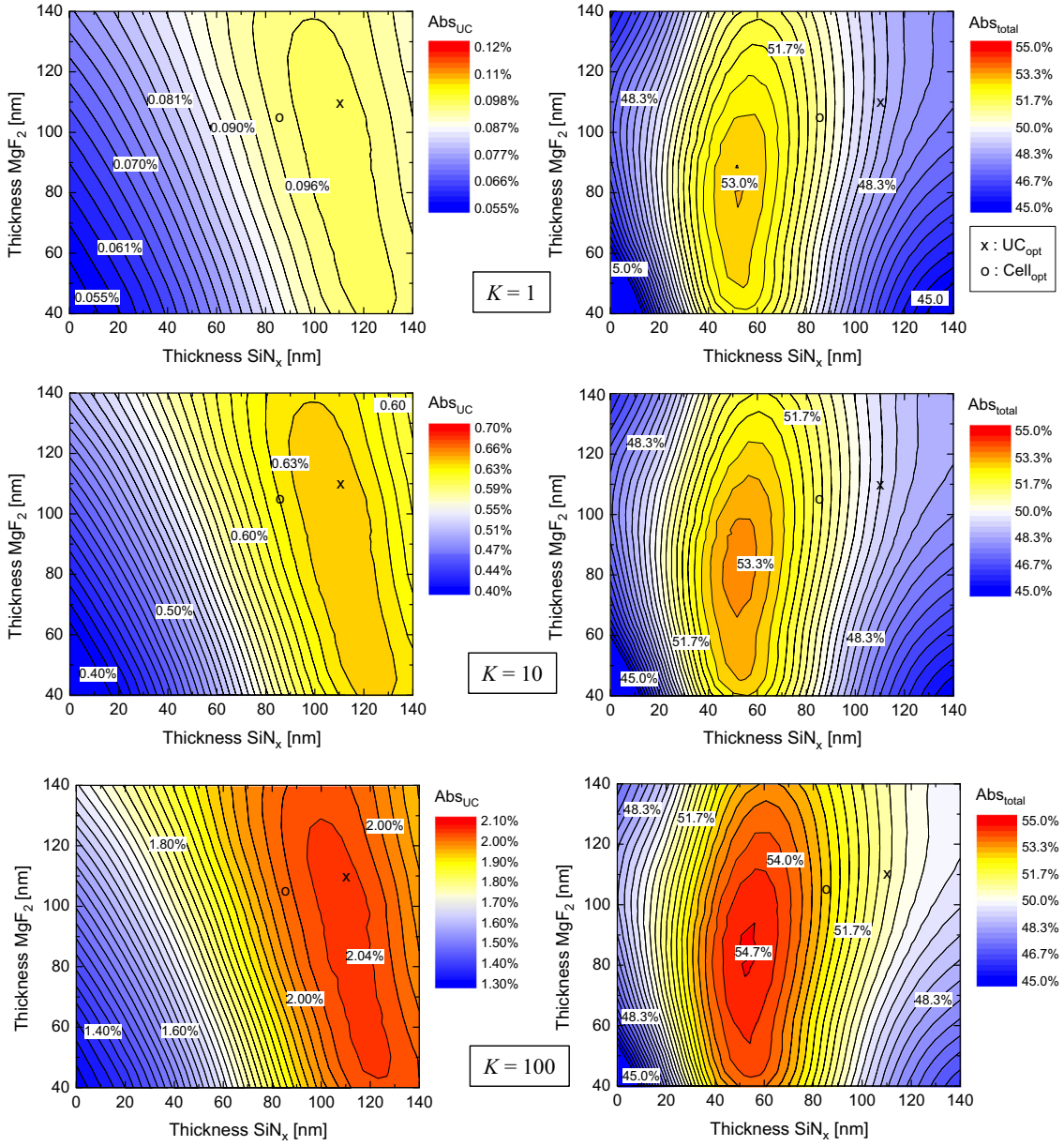

Fig. 3. Impact of the layer thicknesses on Abs_{UC} (left) and Abs_{total} (right) in a a-SiN_x:H and MgF_2 stack as DLARC for the front side of a planar bifacial Si solar cell. Calculations were performed for three different levels of internal spatial concentration ($K=1$, 10, 100). The higher the concentration, the higher are Abs_{UC} and Abs_{total}. The overall impact of Abs_{UC} is small relative to Abs_{total} even for high K, so the optimum layer thicknesses for overall performance do not change significantly from the values determined for the best solar cell performance ($Cell_{opt}$).

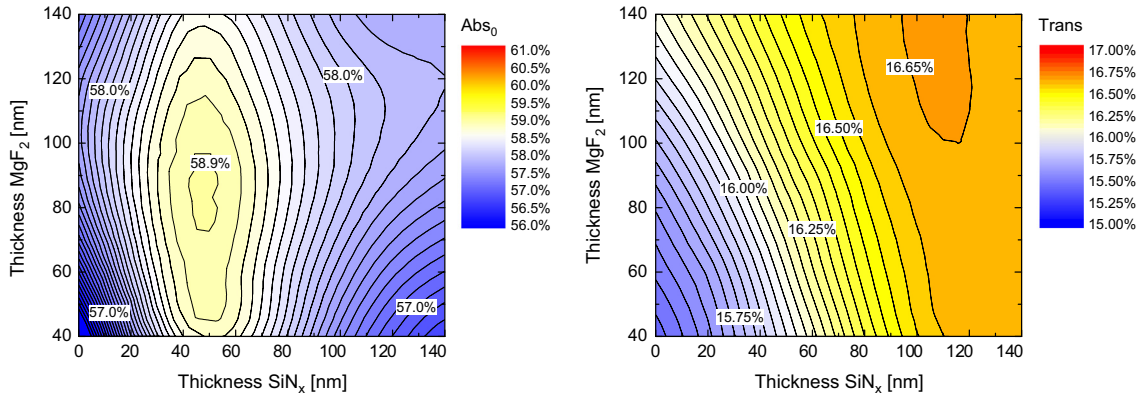

Fig. 4. Optimization of layer thicknesses for a-SiN_x:H/MgF_2 front side DLARC of a bifacial Si solar cell textured on both sides. A higher fraction of photons being directly absorbed in the solar cell Abs_0 is achieved in comparison to the calculations featuring planar solar cells (left), cf. Fig. 2. On the other hand the fraction of transmitted, upconvertible photons *Trans* is decreased (right).

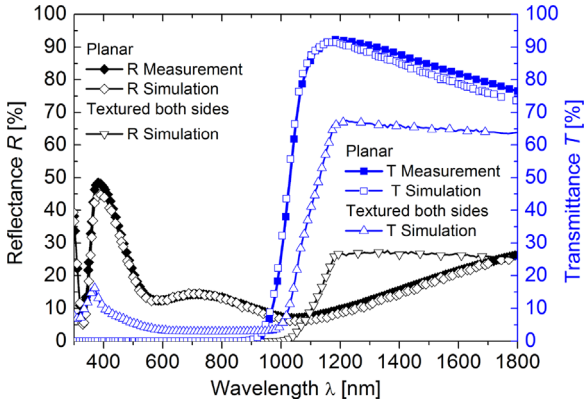

Fig. 5. Comparison of simulated and experimentally measured reflectance $R(\lambda)$ and transmittance $T(\lambda)$ for planar (rectangles) and both-sides-textured (triangles) bifacial Si solar cells featuring MgF_2 on top of a-SiN_x:H as DLARC with the thicknesses of the UC_{opt} scheme (cf. Table 1). The texture reduces reflection in the visible and transmission in the sub-band-gap region.

single-layer, 120 nm a-SiN_x:H ARC was assumed for the rear side. The optimization of the rear side ARC will be discussed after the optimization of the front side in Section 2.3.3.

2.3.1. *Material combination a-SiN_x/MgF_2 on the front of planar solar cells*

Fig. 2 shows the impact of the a-SiN_x:H and MgF_2 layer thicknesses on Abs_0 and *Trans* for planar bifacial Si solar cells. The ARC thicknesses leading to the highest Abs_0 are around 50 nm a-SiN_x:H and 80 nm MgF_2 (Fig. 2, left). With this optimum configuration 52.9% of the incident photons are absorbed directly in the solar cell. In the following, layer systems optimized for the highest Abs_0 will be referred to as "$Cell_{opt}$".

To achieve the highest *Trans* the layers have to be thicker, shifting the reflection minima towards the infrared. As this increases the reflection in the visible, there is a trade-off between optimizing Abs_0 and *Trans*. Fig. 2 (right) indicates the optimum layer thicknesses for the highest *Trans* in the range of 110 nm a-SiN_x and 90 nm MgF_2. About 21.2% of the incidents photons are transmitted through the solar cell and have sufficient energy to be upconverted. Layer systems optimized for the highest *Trans* are denoted as "UC_{opt}" throughout this work.

The overall Abs_{total} depends on the $eUCQY(I_{inc,UC})$, which in turn depends on the chosen spatial concentration ratio *K*. We calculated Abs_{UC} and Abs_{total} for three different scenarios: (i) with $K=1$ (no spatial concentration); (ii) an intermediate concentration of $K=10$; and (iii) an extreme scenario with $K=100$. Although it is not fully realistic to assume that $K=100$ could be reached with the configuration described, this becomes more achievable once external concentration via lenses or mirrors is considered. Fig. 3 shows how the layer thickness variation influences Abs_{UC} and Abs_{total} in the three different scenarios.

With only 0.10% at the maximum position, Abs_{UC} is very low for $K=1$. The main reason is the low irradiance $I_{inc,UC}$ onto the upconverter of around 117 W/m^2. At such a low irradiance the corresponding $eUCQY(I_{inc,UC})$ is only 0.6%. For higher *K* values, Abs_{UC} increases. For example, at $K=100$ Abs_{UC} reaches 2.05% based on an $eUCQY(I_{inc,UC})$ of 12.8%. This still can be considered a realistic value for $eUCQY(I_{inc,UC})$, as comparable values were already determined experimentally for β-$NaY_{0.8}Er_{0.2}F_4$ under high irradiance levels by Richards and Shalav [5]. The overall impact of UC on the system performance is limited, however, as Abs_{UC} is small relative to Abs_{total} even for high *K* values. In consequence, the optimum layer thicknesses for the best overall performance do not change from the values determined for the best solar cell performance ($Cell_{opt}$). For $K=100$, the highest value for Abs_{total}, which is achieved in the $Cell_{opt}$ scheme, is 54.7%. With the corresponding optimum layer thicknesses, Abs_{UC} is 1.74%, representing a relative increase of 3.3% of the overall fraction of absorbed photons due to the added upconverter. The solar cell without the upconverter would have a maximum potential short circuit current density of $J_{sc,0}=36.6$ mA/cm^2, to which the upconverter would add another $J_{sc,UC}$ of 1.2 mA/cm^2.

2.3.2. *Material combination a-SiN_x:H/MgF_2 on front of solar cells textured on both sides*

We carried out a similar analysis for solar cells textured on both sides (see Fig. 4). In comparison to the planar case, Abs_0 increases considerably and reaches an optimum value of 58.9%. The corresponding optimum layer thicknesses are 50 nm of a-SiN_x:H and 90 nm of MgF_2 ($Cell_{opt}$). On the other hand, *Trans* decreases. A maximum of 16.7% is reached for a combination of 100 nm a-SiN_x:H and 140 nm MgF_2 (UC_{opt}). The reason for these differences is that the texture decreases reflection in the visible, which leads to the high Abs_0, but the texture also decreases the transmittance in the relevant UC spectral range, which reduces *Trans*. To highlight these differences the simulated reflectance $R(\lambda)$ and transmittance $T(\lambda)$ of solar cell precursors (with no metallization applied) optimized for the UC_{opt} scenario are shown in Fig. 5. In the case of the planar precursor, experimental results are shown for comparison.

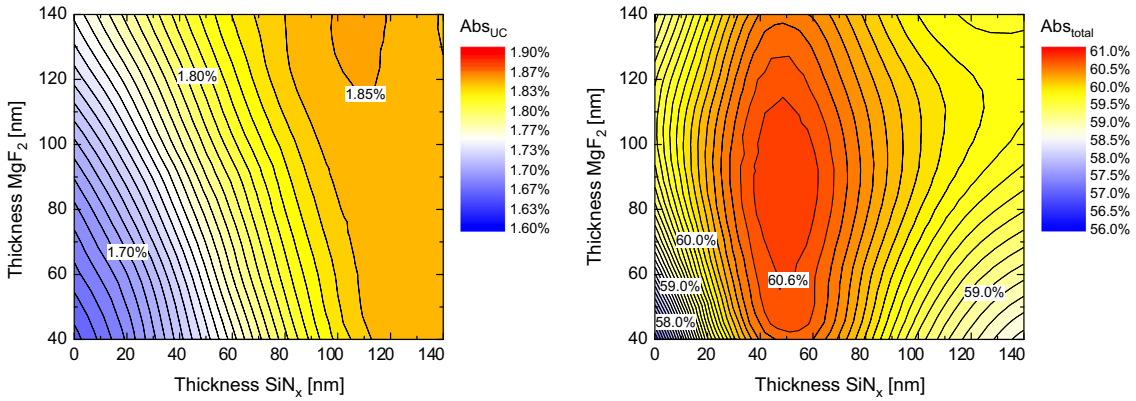

Fig. 6. Impact of the front side a-SiN$_x$ /MgF$_2$ DLARC layer thickness variations on Abs_{UC} and Abs_{total} for a Si solar cell textured on both sides and an internal spatial concentration factor of $K=100$. The maximum Abs_{UC} is 1.85%, while Abs_{total} peaks at 60.7%, corresponding to an overall equivalent short-circuit current density of 40.7 mA/cm^2.

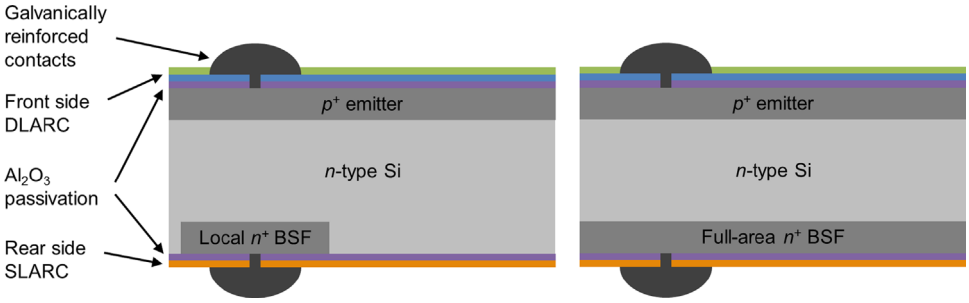

Fig. 7. Schematic of the bifacial Si solar cells produced in this work for UC applications. For simplicity, only the planar devices are depicted here.

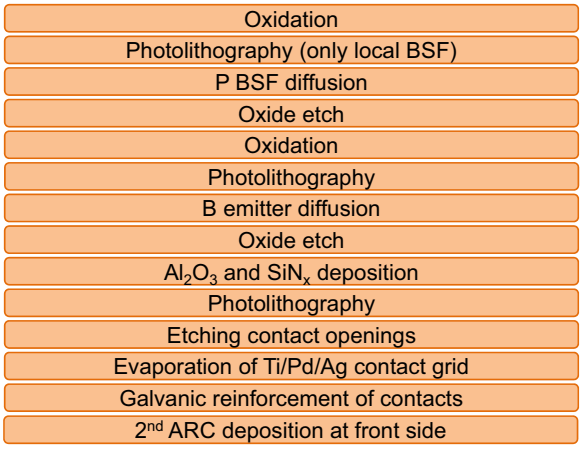

Fig. 8. Overview of the processing sequence for the fabrication of the planar bifacial solar cells.

Fig. 6 shows the impact of the thickness variations on Abs_{UC} and Abs_{total} for the solar cell textured on both sides. Only the case of an internal concentration of $K=100$ is shown, as the dependence on K is qualitatively similar to the one presented for the planar solar cell in Fig. 3. A maximum Abs_{UC} of 1.85% is reached. This is only slightly lower than for the planar case, despite the lower transmission of upconvertible photons, since the upconverted photons are absorbed more efficiently when the rear is textured. The combined value of Abs_{total} has a maximum of 60.7% in the Cell$_{opt}$ scheme, which is considerably higher than for the all planar solar cells. Again, the relative impact of the upconverter is too small to change the optimum layer thicknesses significantly in comparison to the case optimized for the best solar cell performance. At the optimum position the estimated $J_{sc,0}$ is 40.7 mA/cm^2, to which the upconverter could add another $J_{sc,UC}$ of 1.2 mA/cm^2. This corresponds to a relative increase in J_{sc} of 3.0%.

Table 2
Overview of the variation of the double-layer ARCs for the front side of the fabricated solar cells. Two different materials for the 2nd ARC have been used, MgF$_2$ and SiO$_2$, and the layer thicknesses are optimized for both, high upconversion (UC$_{opt}$) and high solar cell efficiencies (Cell$_{opt}$). Due to a processing error, the 1st ARCs were not deposited with the ideal layer thicknesses. Thus, the thicknesses of the 2nd ARCs were adjusted. The ideal values are given in brackets.

Optimization	ARC front side		ARC rear side
	1st ARC	2nd ARC	
UC$_{opt}$	110 (110) nm a-SiN$_x$:H	110 (90) nm MgF$_2$	120 nm a-SiN$_x$:H
Cell$_{opt}$	85 (50) nm a-SiN$_x$:H	105 (80) nm MgF$_2$	120 nm a-SiN$_x$:H
UC$_{opt}$	105 (100) nm a-SiN$_x$:H	105 (100) nm SiO$_2$	120 nm a-SiN$_x$:H
Cell$_{opt}$	75 (50) nm a-SiN$_x$:H	90 (70) nm SiO$_2$	120 nm a-SiN$_x$:H

2.3.3. Rear side anti-reflection coatings

For the optimization of the ARC at the rear side of the solar cell, only the infrared part of the spectrum has to be considered, because the solar cell absorbs the visible light. Consequently, a single layer anti-reflection coating (SLARC) is sufficient. This layer should transmit photons with wavelengths beyond 1150 nm such that they can reach the upconverter. Furthermore, photons being emitted from the upconverter around $\lambda=980$ nm need to be coupled into the solar cell efficiently where the upconverter is attached. For the rest of the solar cell area, the reflection for wavelengths below 1150 nm should be high to increase the path length of the light in the solar cell, thus increasing absorption.

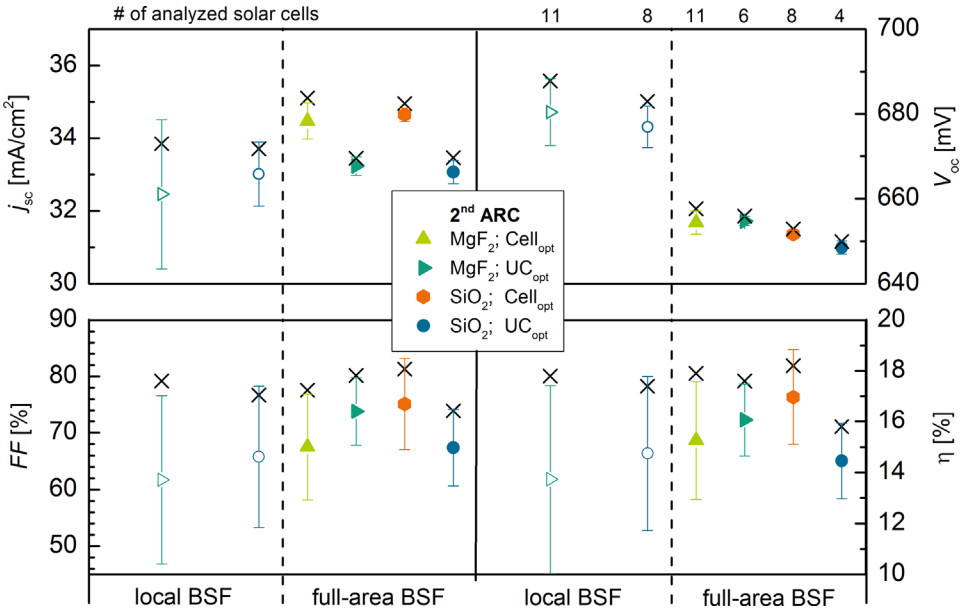

Fig. 9. Overview of the measured solar cell parameters. The planar solar cells vary in thickness and material of the front side anti-reflection coatings. Furthermore, cells with local and full-area BSF were produced. Shown are the arithmetic means, the standard deviations, and the highest achieved value (indicated by a cross), respectively.

However, in the configuration presented in Fig. 1, the function of a rear reflector for photons with wavelengths shorter than 1150 nm is carried out by the spectrally selective photonic structure on top of the LSC and is therefore not considered in the optimizing of the rear SLARC.

For the optimization of the rear surface SLARC, we assumed a refractive index for the adjoining upconverter of $n=1.5$, and a 10 nm-thick Al_2O_3 passivation layer. During the optimization of the rear side, we assumed for the front side coating a layer stack of 90 nm MgF_2/50 nm TiO_2/10 nm Al_2O_3. We found that the most promising SLARC for the rear side of a planar Si solar cell is a 140 nm layer of TiO_2, leading to the highest Abs_{UC} values. Comparable results could be achieved with 120 nm of a-SiN$_x$:H. In the case of a textured solar cell the optimum layer thickness is 120 nm for both TiO_2 and a-SiN$_x$:H.

3. Fabrication of bifacial silicon solar cells

3.1. Fabrication parameters

The realized solar cell structures are shown schematically in Fig. 7. The design is based on the concept presented in 1981 by Cuevas et al. for highly efficient bifacial Si solar cells [40]. However, the solar cells deviate from the original design and feature planar surfaces to maximize the transmission of photons that can be upconverted, thus maximizing the relative impact of the attached upconverter (see Sections 1 and 2). The solar cells were made of 200 μm thick 4 in. wafers of 1 Ω cm *n*-type float zone (FZ) Si base material. On each wafer seven cells were processed with the dimensions of 2 cm × 2 cm.

A sequence of the process steps is shown in Fig. 8. To achieve a deep emitter doping profile with a relatively low surface doping concentration, the wafers were exposed to an additional high-temperature step after boron diffusion. Half of the fabricated solar cell batch features full-area phosphorus diffused n^+ back surface fields (BSF) (Fig. 7, right), whereas the other half features local n^+ BSFs below the contact areas with a width of 30 μm (Fig. 7, left). The boron doped emitter profiles feature a sheet resistance of $R_{sh}=130$ Ω/sq, and the phosphorus doped BSF profiles $R_{sh}=19$ Ω/sq.

For surface passivation, 10 nm thick Al_2O_3 layers were deposited by atomic layer deposition. A DLARC was applied on the front side of the solar cell, using the stacks of a-SiN$_x$:H/MgF_2 and a-SiN$_x$:H/SiO_2. Stacks containing TiO_2 caused problems during the etching of the contact openings, and no working solar cells could be realized using TiO_2. Layers of different thicknesses were deposited, optimized for UC$_{opt}$ or Cell$_{opt}$, as discussed in Section 2. The variations and ARC thicknesses are summarized in Table 2. The first ARC layers of both surfaces were deposited before metallization. Photolithography and wet etching was subsequently used to create openings for the contacts in these layers. The second ARC layer on the front side of the solar cells was applied after metallization, consisting of PECVD SiO_2 or evaporated MgF_2, respectively. For the SLARC of the rear side a a-SiN$_x$:H layer with a thickness of 120 nm was applied.

To achieve the bifacial functionality and low shading losses of the solar cell, the front and rear sides feature aligned finger grids. The contact finger distance is 800 μm. The contact fingers consist of a titanium/palladium/silver (Ti/Pd/Ag) stack, deposited after the etch-back process of the first ARC layer. At this point, the metal grid fingers are only 8 μm wide and have a height of 0.2 μm. This metal seed layer is then thickened by Ag electroplating. With this process sequence, it is possible to obtain contacts with a good aspect ratio of height and width, featuring both relatively low shading losses and low lateral series resistance losses [41]. However, because the bifacial solar cells do not feature an entire rear surface metallization the electrical potential during the plating tends to be inhomogeneous, resulting in a relatively large standard deviation of the plating thickness of 9 μm for the solar cells with local BSF at an average plating thickness of 15 μm. The solar cells featuring a full-area BSF were less affected, due to the enhanced lateral conductivity of the phosphorus doping at the rear side with an average plating thickness of 12 ± 5 μm. Reduced electro-plating results in too thin contact fingers, and too thick Ag layer may cause adhesion problems of the metal finger, both leading to larger series resistance.

3.2. Resulting solar cell performance

We were especially interested in how the variations of the ARC parameters (see Table 2) and the different BSF configurations

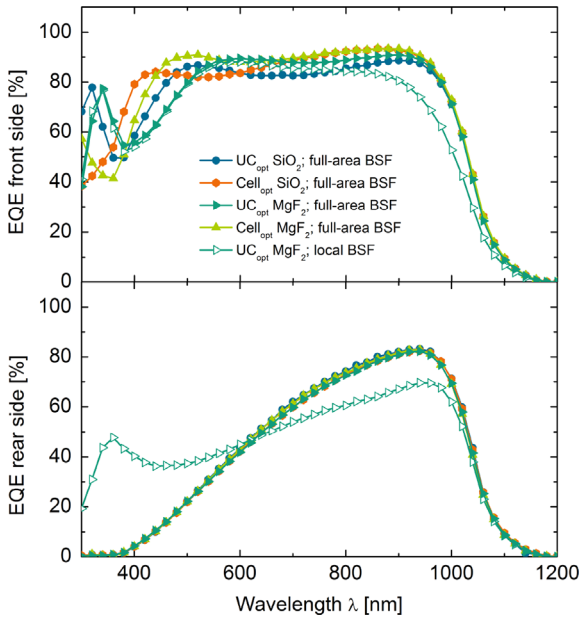

Fig. 10. *EQE* measured from the front (top) and rear (bottom) of the solar cells used in the later UC PV device measurements. The solar cells differ in the second layer of the DLARC (SiO_2 or MgF_2), and the BSF layout (local or full-area). The data for the *EQE* of the rear side for the Cell$_{opt}$ SiO_2: full-area BSF solar cell were measured on a solar cell similar to the one used, as the original was not available for the rear side EQE measurements any more.

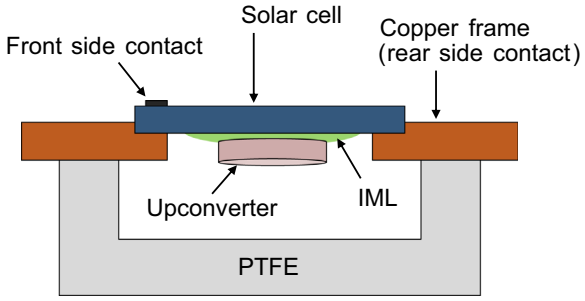

Fig. 11. Schematic of the measurement chuck used for upconversion measurements. The upconverter was coupled directly to the solar cell via the IML.

affect the electrical solar cell parameters. The measurement results are summarized in Fig. 9. For each variation four to eleven solar cells were available for statistical analysis. The numbers at the top of the upper graph indicate how many solar cells were analyzed in the specific variation. The average values, the maximum values and the standard deviations for each variation are shown as well.

The different optimizations of the ARCs, either for high upconversion (UC$_{opt}$) or high solar cell efficiency (Cell$_{opt}$), are reflected in the results of the J_{sc}, see Fig. 9. As expected from the discussion in Section 2, the Cell$_{opt}$ optimized solar cells featuring thinner ARCs show higher J_{sc} values than the UC$_{opt}$ optimized solar cells. Fig. 10 displays the EQE measured from front and rear side of the solar cell, for the best solar cell of each kind that were subsequently used in the measurements with attached upconverter. Corresponding to the thinner layer thicknesses, a first local maximum of the EQE from the front occurs at shorter wavelengths in the Cell$_{opt}$ scheme. No impact of the different front DLARC is found in the EQE from the rear. Also, no significant benefit of the MgF_2 layer with $n=1.39$ over the ARC made with SiO_2 with $n=1.47$ was observed. The solar cells with local BSF achieve much higher V_{oc} values. The maximum values of comparable solar cells with local BSFs are about 30 mV higher than for solar cells featuring full-area BSFs. Such a difference is also found in numerical simulations of the different structures. However, the scattering of the results, reflected in the large standard deviation, is significantly larger for the solar cells with local BSF. Possible reasons are not properly diffused or misaligned local diffusion regions, and inhomogeneous electro-plating. In consequence, the use of local BSFs might be the most promising, but also more fragile approach. The local BSF also affects the EQE from the rear. Here, a higher performance is observed for short wavelengths, which has, however, no impact on the performance of the UC PV device. In contrast, at long wavelengths in the emission region of the upconverter the EQE from the rear is reduced, which is detrimental for the UC PV device performance (which we will see in the following section).

4. Measurements of bifacial solar cells with upconverter

4.1. Method and setup for external quantum efficiency measurements of solar cells with attached upconverter

We investigated the performance of the different bifacial Si solar cells with an upconverter sample attached to the rear side of the solar cell. For this purpose, the solar cells featuring the highest efficiencies of each of the produced variations were chosen (see Figs. 9 and 10). The solar cells were soldered to a copper frame and placed on top of a polytetrafluoroethylene (PTFE) chuck with a recess for the upconverter for the measurements, as depicted in Fig. 11.

Microcrystalline β-$NaY_{0.8}Er_{0.2}F_4$ [16] powder was embedded in the polymer perfluorocyclobutyl (PFCB, Tetramer Inc.), with a polymer to upconverter weight ratio of 84.9 w/w% to form a solid disk (dimensions: 12.5 mm diameter and 1 mm thick) [42]. Additionally a reference sample with un-doped β-$NaYF_4$ was fabricated. The refractive index of the PFCB is 1.52 at 1500 nm [43]. The same upconverter sample was used in all experiments. In these experiments, the embedded upconverter was optically coupled to the solar cell by an index matching liquid (IML) and hold in place just with surface tension. The IML was immersion oil (Type 300, Cargille Laboratories) with a refractive index of $n=1.52$ at the longest specified wavelength of $\lambda=656$ nm.

The solar cell upconverter device was illuminated by a tunable near infrared laser (ECL-210, Santec). The laser output was not stable at $\lambda=1523$ nm (where the highest upconversion quantum yield is observed [6]), so 1508 nm stable excitation was used since it is known that this wavelength exhibits 90% of the external upconversion quantum yield of β-$NaY_{0.8}Er_{0.2}F_4$ compared to 1523 nm [6]. To determine the irradiance onto the solar cell, the incident photon flux was determined as a function of the laser power with a germanium reference solar cell, of which the EQE_{Ge} is known with an uncertainty of 1% absolute. The illuminated area of the laser beam was measured with an InGaAs camera (Xeva InGaAs, Xenics) to have a full area at half maximum of $A_{laser}=(3.4\pm0.3)$ mm^2 at the sample position. During the measurements, the short-circuit current I_{SC} of the solar cells was recorded without bias illumination. In order to deduce the *EQE* of the upconverter solar cell device, the short-circuit currents of the solar cell with attached upconverter $I_{SC,UC}$, with attached reference sample $I_{SC,ref}$ and of the reference germanium solar cell $I_{SC,Ge}$ were measured under the same illumination conditions. The EQE_{UC} can then be calculated via

$$EQE_{UC}(\lambda,I)=EQE_{Ge}(\lambda)\frac{I_{SC,UC}(\lambda,I)-I_{SC,ref}(\lambda,I)}{I_{SC,Ge}(\lambda,I)}. \quad (9)$$

as upconversion is a non-linear process, the EQE_{UC} does not only depend on the wavelength λ, but also on the incident irradiance I of the laser.

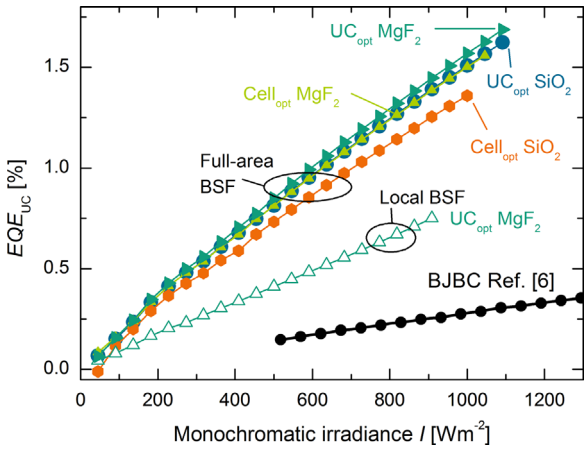

Fig. 12. EQE_{UC} at $\lambda=1508$ nm of Si UC PV devices as a function of monochromatic irradiance I for different types of solar cells to which the same upconverter sample was attached on the rear side. The adapted EQE_{UC} of an UC PV device with BCBJ Si solar cell not optimized for UC from Ref. [6] is plotted as well.

4.2. Results

Measurements of the EQE_{UC} in dependence on the excitation irradiance were carried out for the different types of solar cells. The results are summarized in Fig. 12. For comparison, the results of Fischer et al. [6] using a planar bifacial Si back-junction back-contact (BJBC) solar cell [44] are shown as well. The excitation wavelength of the laser used in these experiments had been $\lambda=1523$ nm. For comparison with the results achieved with our optimized bifacial solar cells we scaled the values from Ref. [6] by a factor of 0.9, accounting for the lower external upconversion quantum yield at an excitation wavelength of 1508 nm.

For the planar solar cells optimized and realized in this work, the achieved EQE_{UC} values are significantly higher than those reported in Ref. [6]. For an UC_{opt} solar cell with a MgF_2 ARC coating and a full-area BSF we reached an EQE_{UC} of 1.69% for a monochromatic irradiance of 1091 W/m^2. This corresponds to a value of 0.15 (W/cm^2)$^{-1}$, when normalized to the incident irradiance I. Compared to the value of Shalav et al. of 0.014 (W/cm^2)$^{-1}$ [8] and the value of Fischer et al. of 0.03 (W/cm^2)$^{-1}$ [6], one can see the considerable increase by a factor of five compared to the best published values so far for using non-optimized solar cells.

Significant differences are visible for the different types of solar cells. From theoretical considerations, we would expect that the EQE_{UC} is mainly determined by the transmission of the solar cell at $\lambda=1508$ nm and, to a lesser extent, by the EQE at 980 nm for rear side illumination. Therefore the different configurations for the ARCs should have the strongest impact. We see, however, the biggest differences are found between systems featuring solar cells with local BSF on the one hand and full-area BSF on the other hand. In Table 3 all measured solar cells are listed with the corresponding measured EQE under illumination from the rear side of the solar cells at 980 nm and the transmittance values at a wavelength of 1508 nm, respectively. As can be seen in Table 3, the transmittance of the solar cell featuring local BSF is comparable to those of solar cells with full-area BSF. In contrast, the EQE value under illumination from the rear is significantly lower. Furthermore, the EQE values given in Table 3 are determined with the use of bias light with an intensity of about one sun, whereas the irradiation emitted from the upconverter is less than 0.01 suns and only a few mm^2 of the solar cell are illuminated. At these low irradiation intensities, the rear side recombination with local BSF increases significantly, caused by a reduced surface passivation of the Si surface with Al_2O_3 due to the low minority carrier density [45,46]. In consequence, the EQE from the rear under the UC measurement conditions for the local-area BSF solar cell should be even worse than indicated by the displayed numbers. On the other hand, in solar cells featuring full-area BSF, there is not such a strong dependence of the surface passivation on the illumination intensity, and hence the superior performance is observed.

Table 3
Overview of the bifacial solar cells, on which the EQE_{UC} measurements were performed, as shown in Fig. 12. Given are the EQE under illumination from the rear side of the solar cells at $\lambda=980$ nm, as well as the transmittance at an excitation wavelength of $\lambda=1508$ nm.

	BSF	*2nd front ARC*	Rear side *EQE* at $\lambda=980$ nm (%)	Transmittance at $\lambda=1508$ nm (%)
BCBJ[a]	n/a	n/a	~76	(40 ± 5)[b]
UC_{opt}	Full-area	MgF_2	76.8	84.2
UC_{opt}	Full-area	SiO_2	78.2	82.1
$Cell_{opt}$	Full-area	MgF_2	76.9	80.8
$Cell_{opt}$	Full-area	SiO_2	78.2[c]	72.4[c]
UC_{opt}	Local	MgF_2	67.7	84.8

[a] Data from Ref. [44].
[b] Transmittance at 1523 nm.
[c] Measured at a solar cell similar to the one used in the measurement for EQE_{UC}.

In addition, from Fig. 12 we can see that the solar cells having ARCs following the UC_{opt} scheme tend to lead to a higher EQE_{UC} than the solar cells featuring the $Cell_{opt}$ scheme. From Table 3, we can see that for the solar cells with full-area BSF the same relative order as for the EQE_{UC} values can be found in the transmittance values, as expected. The variations of the transmittance are caused on the one hand by the different thicknesses of the anti-reflection coatings for UC_{opt} and $Cell_{opt}$, and on the other hand by different shading losses caused by the contact fingers. Simulations show that due to the varying plating thicknesses, the shading losses of the solar cells may vary by about 2%. At 1508 nm, the material of the uppermost front ARC, being SiO_2 or MgF_2, respectively, has only a minor influence on the transmission of the solar cells, which is negligible compared to the effect of the contact grid.

5. Conclusions

In this paper, we optimized front and rear ARCs of bifacial Si solar cells for the application of upconverter materials, to harvest also sub-band-gap photons. We defined three figures-of-merit for an UC PV device, being the absorptance in the solar cell without upconverter, the transmittance of upconvertible photons through the solar cell, and the overall absorptance of photons in the solar cell when an upconverter is attached to its rear side. For the calculation of the overall absorptance, the performance of the solar cell, as well as the transmittance of upconvertible photons, the quantum yield by which these photons are upconverted, and the absorption of the upconverted photons by the solar cell were modeled. We used the model to optimize ARCs on the front and the rear surface of the device, and to estimate the potential of UC based on realistic solar cell models and experimental upconverter data, assisted by some idealistic assumptions of how the spectral range contributing to UC could be extended. The optimization of the front side ARC showed that there is a trade-off between optimizing the solar cell performance and maximizing the impact of the upconverter. The impact of the upconverter on the overall device performance is, however, much smaller than the impact of the solar cell. Hence for highest overall performance the solar cell performance should be optimized. For the same reason, both side textured solar cells with attached upconverter have a much higher overall potential than planar solar cells. For these solar cells the lower transmission of upconvertible photons is over-compensated by lower

reflection in the visible spectral region and better absorption of photons with energies slightly above the band-gap of Si.

The highest potential was found for a bifacial Si solar cell textured on both surfaces with a DLARC consisting of 40 nm of a-SiN_x:H and 80 nm of SiO_2 on the front surface, and a 120 nm a-SiN_x:H ARC at the rear surface. The fraction of absorbed photons calculated for such an optimized solar cell corresponds to a maximum possible short-circuit current density of the solar cell without the upconverter of 40.8 mA/cm^2 to which the upconverter could add another 1.2 mA/cm^2, thus resulting in a relative increase of 3.0%. An alternative material system for the front DLARC with a-SiN_x:H and MgF_2 showed a very similar potential, while the system of TiO_2 and MgF_2 has a slightly lower potential especially on planar wafers. These results are based on the assumption of the use of a second luminescent material extending the utilized spectral range, as well as concentrating light onto the upconverter.

Our calculations show that concentration is very important for achieving a significant impact of the upconverter. From this one could conclude that the 3% relative increase constitutes an upper limit on what can be achieved with realistic upconverter materials. On the other hand, our analysis was based on measured upconversion quantum yield values. As an example, for a monochromatic irradiance of 1050 W/m^2 an $eUCQY(I_{inc,UC})$ of 3.7% was assumed. In the meantime, values as high as an eUCQY of 6.5% were observed using a quite similar monochromatic irradiance of 1100 W/m^2 at 1510 nm for Gd_2O_2S: 10% Er^{3+} [47], nearly doubling the performance assumed in the presented calculations. So to achieve the same impact on the overall device performance, the idealized assumption could be relaxed to rather realistic levels, when the new UC material properties are taken into account. Furthermore, additional concepts to enhance UC performance, like plasmonics or photonic structures were not considered, which might enable even higher upconverter performance. One could also imagine the application of upconversion in III–V silicon tandem solar cell structures, where the silicon solar cell delivers a lower current, and thus, for a given UC performance, the relative impact would be higher. These systems have the additional benefit of usually being operated under external concentration, which further increases UC performance.

Experimentally, we realized planar, bifacial monocrystalline *n*-type Si solar cells with different optimized ARC schemes and BSF configurations. Solar cell structures with a local BSF yielded higher maximum open-circuit voltages in comparison to structures with a full area BSF. However, the processing of solar cells with local back surface field was more fragile and scatter within the results was higher, especially for the fill factor. Due to worse performance under low illumination conditions, no benefit from a local BSF was observed in the UC measurements. ARCs optimized for highest UC efficiency lead indeed to a higher EQE_{UC} of the upconverter solar cell device, than coatings optimized for highest solar cell performance. We found that optimized front ARCs made of a-SiN_x:H/SiO_2 had similar high performance to a-SiN_x:H/MgF_2 stacks. For the best realized UC PV device, featuring MgF_2 as a second layer, we determined an EQE_{UC} of 1.69% at 1508 nm with an irradiance of 1091 W/m^2. Normalized to the irradiance, the value is 0.15 (W/cm^2)$^{-1}$, which constitutes a five-fold increase in comparison to the highest normalized value published so far that were achieved with non-optimized solar cells.

Acknowledgments

The research leading to these results has received funding from the European Community's Seventh Framework Programme (FP7/2007–2013) under Grant agreement no. [246200] within the "Nanospec" project. Stefan Fischer gratefully acknowledges the scholarship support from the Deutsche Bundesstiftung Umwelt DBU. Jan Christoph Goldschmidt gratefully acknowledges the scholarship support from the German Academic Exchange Service DAAD.

Appendix A. Supplementary material

Supplementary data associated with this article can be found in the online version at http://dx.doi.org/10.1016/j.solmat.2014.05.014.

References

[1] T. Trupke, A. Shalav, B.S. Richards, P. Würfel, M.A. Green, Efficiency enhancement of solar cells by luminescent up-conversion of sunlight, Sol. Energy Mater. Sol. Cells 90 (2006) 3327–3338.
[2] P. Gibart, F. Auzel, J.C. Guillaume, K. Zahraman, Below band-gap IR response of substrate-free GaAs solar cells using two-photon up-conversion, Jpn. J. Appl. Phys. 35 (1996) 4401–4402.
[3] J.C. Goldschmidt, P. Loper, S. Fischer, S. Janz, M. Peters, S.W. Glunz, G. Willeke, E. Lifshitz, K. Krämer, D. Biner, Advanced upconverter systems with spectral and geometric concentration for high upconversion efficiencies, in: Proceedings of the IUMRS International Conference on Electronic Materials, Sydney, Australia, 2008, pp. 307–311.
[4] C.M. Johnson, G.J. Conibeer, Limiting efficiency of generalized realistic c-Si solar cells coupled to ideal up-converters, J. Appl. Phys. 112 (2012).
[5] B.S. Richards, A. Shalav, Enhancing the near-infrared spectral response of silicon optoelectronic devices via up-conversion, IEEE Trans. Electron Devices 54 (2007) 2679–2684.
[6] S. Fischer, J.C. Goldschmidt, P. Loper, G.H. Bauer, R. Brüggemann, K. Krämer, D. Biner, M. Hermle, S.W. Glunz, Enhancement of silicon solar cell efficiency by upconversion: optical and electrical characterization, J. Appl. Phys. 108 (2010) 044912.
[7] J.C. Goldschmidt, S. Fischer, P. Loper, K.W. Krämer, D. Biner, M. Hermle, S. W. Glunz, Experimental analysis of upconversion with both coherent monochromatic irradiation and broad spectrum illumination, Sol. Energy Mater Sol. Cells 95 (2011) 1960–1963.
[8] A. Shalav, B.S. Richards, M.A. Green, Luminescent layers for enhanced silicon solar cell performance: up-conversion, Sol. Energy Mater. Sol. Cells 91 (2007) 829–842.
[9] F. Auzel, Upconversion and anti-stokes processes with f and d ions in solids, Chem. Rev. 104 (2004) 139–173.
[10] B. Ahrens, P. Loper, J.C. Goldschmidt, S.W. Glunz, B. Henke, P.-T. Miclea, S. Schweizer, Neodymium-doped fluorochlorozirconate glasses as an upconversion model system for high efficiency solar cells, Phys. Status Solidi A 205 (2008) 2822–2830.
[11] J. Zhao, M.A. Green, Optimized antireflection coatings for high-efficiency silicon solar cells, IEEE Trans. Electron Devices 48 (1991) 1925–1934.
[12] C.M. Garner, F.W. Sexton, R.D. Nasby, High-efficiency silicon solar cells for luminescent solar concentrators, Sol. Cells 4 (1981) 37–46.
[13] K.R. McIntosh, G. Lau, J.N. Cotsell, K. Hanton, D.L. Baetzner, F. Bettiol, B. S. Richards, Increase in external quantum efficiency of encapsulated silicon solar cells from a luminescent down-shifting layer, Prog. Photovolt. 17 (2009) 191–197.
[14] A. Shalav, B.S. Richards, T. Trupke, R.P. Corkish, K.W. Krämer, H.U. Güdel, M.A. Green, The application of up-converting phosphors for increased solar cell conversion efficiencies, in: K. Kurokawa, L.L. Kazmerski, B. McNelis, M. Yamaguchi, C. Wronski, W.C. Sinke (Eds.) Proceedings of the 3rd World Conference on Photovoltaic Energy Conversion, WCPEC-3 Organizing Committee, December 2003, Osaka, Japan, 2003, pp. 248–250.
[15] A. Shalav, B.S. Richards, T. Trupke, K.W. Krämer, H.U. Güdel, Application of $NaYF_4$:Er^{3+} up-converting phosphors for enhanced near-infrared silicon solar cell response, Appl. Phys. Lett. 86 (2005) 13505.
[16] K.W. Krämer, D. Biner, G. Frei, H.U. Güdel, M.P. Hehlen, S.R. Lüthi, Hexagonal sodium yttrium fluoride based green and blue emitting upconversion phosphors, Chem. Mater. 16 (2004) 1244–1251.
[17] C. Strümpel, M. McCann, G. Beaucarne, V. Arkhipov, A. Slaoui, V. Švrček, C. Del Cañizo, I. Tobias, Modifying the solar spectrum to enhance silicon solar cell efficiency—an overview of available materials, Sol. Energy Mater. Sol. Cells 91 (2007) 238–249.
[18] J.C. Goldschmidt, P. Loper, M. Peters, Solarelement mit gesteigerter Effizienz und Verfahren zur Effizienzsteigerung, 2007.
[19] Sentaurus TCAD, Release E-2010.12, Synopsys, Zürich, Switzerland, 2010.
[20] M. Hermle, F. Granek, O. Schultz, S.W. Glunz, Analyzing the effects of front-surface fields on back-junction silicon solar cells using the charge-collection probability and the reciprocity theorem, J. Appl. Phys. 103 (2008) 054507.
[21] F. Granek, M. Hermle, D. Huljic, O. Schultz-Wittmann, S.W. Glunz, Enhanced lateral current transport via the front n^+ diffused layer of n-type high-efficiency back-junction back-contact silicon solar cells, Prog. Photovolt.: Res. Appl. 17 (2008) 47–56.
[22] S. Kluska, F. Granek, M. Rüdiger, M. Hermle, S.W. Glunz, Modeling and optimization study of industrial n-type high-efficiency back-contact back-junction silicon solar cells, Sol. Energy Mater. Sol. Cells 94 (2010) 568–577.

[23] M. Rüdiger, C. Schmiga, M. Rauer, M. Hermle, S.W. Glunz, Optimisation of industrial n-type silicon solar cells with aluminum-alloyed rear emitter by means of 2D numerical simulation, in: Proceedings of the 25th European Photovoltaic Solar Energy Conference and Exhibition, Valencia, Spain, 2010, pp. 2280–2286.
[24] F. Kiefer, C. Ulzhofer, T. Brendemühl, N.-P. Harder, R. Brendel, V. Mertens, S. Bordihn, C. Peters, J.W. Müller, High efficiency n-type emitter-wrap-through silicon solar cells, IEEE J. Photovolt. 1 (2011) 49–53.
[25] M. Rüdiger, C. Schmiga, M. Rauer, M. Hermle, S.W. Glunz, Efficiency potential of n-type silicon solar cells with aluminum-doped rear p^+ emitter, IEEE Trans. Electron Devices 59 (2012) 1295–1303.
[26] J. Frank, M. Rüdiger, S. Fischer, J.C. Goldschmidt, M. Hermle, Optical Simulation of bifacial solar cells, Energy Procedia 27 (2012) 300–305.
[27] J. Frank, Simulation von bifacialen Solarzellen für Photovoltaiksysteme mit Hochkonvertern, in: Fakultät für Mathematik und Physik, Universität Freiburg, Freiburg, Germany, 2012, p. 123.
[28] A.C. Atre, J.A. Dionne, Realistic upconverter-enhanced solar cells with non-ideal absorption and recombination efficiencies, J. Appl. Phys. 110 (2011) 034505.
[29] S. Fischer, A. Ivaturi, B. Frohlich, M. Rüdiger, A. Richter, K.W. Krämer, B. S. Richards, J.C. Goldschmidt, Upconverter silicon solar cell devices for efficient utilization of sub-band-gap photons under concentrated solar radiation, IEEE J. Photovolt. 4 (1) (2013) 183–189.
[30] S. Fischer, B. Frohlich, H. Steinkemper, K.W. Krämer, J.C. Goldschmidt, Absolute upconversion quantum yield of β-$NaYF_4$ doped with Er^{3+} and external quantum efficiency of upconverter solar cell devices under broad-band excitation considering spectral mismatch corrections, Sol. Energy Mater. Sol. Cells 122 (2014) 197–207.
[31] K. Jaeger, G. Bende, W. Hoffmann, R. Hezel, Performance of bifacial MIS-inversion layer solar cells encapsulated in novel albedo collecting modules, in: Proceedings of the 23rd IEEE Photovoltaic Specialists Conference, Louisville, Kentucky, USA, 1993, pp. 1235–1239.
[32] IEC, Photovoltaic Devices – Part 3: Measurement Principles for Terrestrial Photovoltaic (PV) Solar Devices With Reference Spectral Irradiance Data., 2nd ed., International Electrotechnical Commission, 2008.
[33] M.A. Green, Silicon Solar Cells: Advanced Principles and Practice, Centre for Photovoltaic Devises and Systems UNSW, Sydney, Australia, 1995.
[34] R.E. Thoma, G.M. Herbert, H. Insley, C.F. Weaver, Phase equilibria in the system sodium fluoride–yttrium fluoride, Inorg. Chem. 2 (1963) 1005–1012.
[35] S.K.W. MacDougall, A. Ivaturi, J. Marques-Hueso, K.W. Krämer, B.S. Richards, Ultra-high photoluminescent quantum yield of β-$NaYF_4$: 10% Er^{3+} via broad-band excitation of upconversion for photovoltaic devices, Opt. Express 20 (2012) A879–A887.
[36] J. Benick, A. Richter, T.-A. Li, N.E. Grant, K.R. McIntosh, Y. Ren, K.J. Weber, M. Hermle, S.W. Glunz, Effect of a post-deposition anneal on Al_2O_3/Si interface properties, in: Proceedings of the 35th IEEE Photovoltaic Specialists Conference, Honolulu, Hawaii, USA, 2010.
[37] J. Benick, B. Hoex, M.C.M. van de Sanden, W.M.M. Kessels, O. Schultz, S. W. Glunz, High efficiency n-type Si solar cells on Al_2O_3-passivated boron emitters, Appl. Phys. Lett. 92 (2008) (253504/253501-253503).
[38] J. Schmidt, F. Werner, B. Veith, D. Zielke, S. Steingrube, P.P. Altermatt, S. Gatz, T. Dullweber, R. Brendel, Advances in the surface passivation of silicon solar cells, in: Proceedings of International Conference on Materials for Advanced Technologies, 2011, pp. 30–39.
[39] G. Dingemans, R. Seguin, P. Engelhart, M.C.M. van den Sanden, W.M. M. Kessels, Silicon surface passivation by ultrathin Al_2O_3 films synthesized by thermal and plasma atomic layer deposition, Phys. Status Solidi RRL 4 (2010) 10–12.
[40] A. Cuevas, J. Eguren, E. Sánchez, M. Cid, Influence of the junction area to edge area ratio on the open-circuit voltage of silicon solar cells, IEEE Trans. Electron Devices ED-28 (1981) 1554–1555.
[41] S. Greil, Charakterisierung und Optimierung der lichtinduzierten Galvanik (LIP) von Silber zur Verstärkung der Vorderseitenkontakte an kristallinen Siliciumsolarzellen, Technische Universität Bergakademie Freiberg, 2008, p. 121.
[42] A. Ivaturi, S.K.W. MacDougall, R. Martín-Rodríguez, M. Quintanilla, J. Marques-Hueso, K.W. Krämer, A. Meijerink, B.S. Richards, Optimizing infrared to near infrared upconversion quantum yield of β-$NaYF_4$:Er^{3+} in fluoropolymer matrix for photovoltaic devices, J. Appl. Phys. 114 (2013) 013505.
[43] Y.K. Olsson, G. Chen, R. Rapaport, D.T. Fuchs, V.C. Sundar, J.S. Steckel, M. G. Bawendi, A. Aharoni, U. Banin, Fabrication and optical properties of polymeric waveguides containing nanocrystalline quantum dots, Appl. Phys. Lett. 85 (2004) 4469.
[44] A. Mohr, T. Roth, S.W. Glunz, BICON: high concentration PV using one-axis tracking and silicon concentrator cells, Prog. Photovolt.: Res. Appl. 14 (2006) 663–674.
[45] B. Hoex, J. Schmidt, P. Pohl, M.C.M. van de Sanden, W.M.M. Kessels, Silicon surface passivation by atomic layer deposited Al_2O_3, J. Appl. Phys. 104 (2008) 044903.
[46] S. Steingrube, P.P. Altermatt, D. Zielke, F. Werner, J. Schmidt, R. Brendel, Reduced passivation of silicon surfaces at low injection densities caused by H-induced defects, in: Proceedings of the 25th European Photovoltaic Solar Energy Conference and Exhibition, Valencia, Spain, 2010, pp. 1748–1754.
[47] R. Martín-Rodríguez, S. Fischer, A. Ivaturi, B. Fröhlich, K.W. Krämer, J. C. Goldschmidt, B.S. Richards, A. Meijerink, Highly Efficient IR to NIR Upconversion in Gd_2O_2S: Er^{3+} for Photovoltaic Applications, Chem. Mater. 25 (2013) 1912–1921.